Green Hydrothermal Synthesis of $Ag@Ag_2O@GO$ Nanocomposites Using Diospyros Kaki Fruit Extract and Their Application in Supercapacitors

Ayşe Bütün
Duzce University
Kübra Zenkin
kubrazenkin@gmail.com
Duzce University
Deniz Emre
Çanakkale Onsekiz Mart University
Sefa Durmuş
Duzce University
Selehattin Yılmaz
Çanakkale Onsekiz Mart University

Research Article

Keywords: Graphene Oxide, Ag NPs, Diospyros kaki, Green Hydrothermal Method, Supercapacitor

Posted Date: January 29th, 2026

DOI: https://doi.org/10.21203/rs.3.rs-8599814/v1

Additional Declarations: No competing interests reported.

Abstract

Increasing global energy demand and environmental concerns have heightened interest in supercapacitors offering high power density and long cycle life. In this context, the synergistic effect of graphene oxide (GO) and silver nanoparticles (AgNPs) plays a significant role in the development of electrode materials. In this study, an eco-friendly $Ag@Ag_2O@GO$ nanocomposite was successfully synthesized via a one-step hydrothermal method using *Diospyros kaki* (*D. kaki)* fruit extract as a reducing and stabilizing agent. The structural and morphological properties of the synthesized nanocomposite were characterized in detail using FTIR, UV-VIS, XRD, SEM-EDX, and TEM analyses. The electrochemical performance of the material as a supercapacitor electrode was evaluated using the CV technique. The obtained results demonstrate a significant specific capacitance of 125.5 F g^{-1} for the $Ag@Ag_2O@GO$ nanocomposite compared to 58.3 F g^{-1} for pure GO, revealing that this structure, synthesized with plant extract, is a potential candidate for advanced energy storage applications.

1. INTRODUCTION

In recent years, energy shortages and global warming have increased the demand for supercapacitors as green energy storage devices [1]. Supercapacitors are energy storage systems that provide high power density, long-term stability, and the capability for rapid charging and discharging [2]. They are preferred primarily due to their higher energy storage capacity compared to conventional capacitors, as well as their environmental friendliness, safety, and reliable operation at high temperatures [3, 4]. Power backup systems, portable devices, electric vehicles, and many other energy storage applications that require short-term, safe, and reliable charging cycles have attracted significant attention in both academic and industrial fields [5, 6]. Supercapacitors can be used independently or in combination with fuel cells and batteries. The major advantages of supercapacitors include their use as power sources in hybrid electric vehicles, flexible electronic devices, backup power systems, voltage stabilizers, and laptops [7]. Research on supercapacitors has focused on enhancing energy density without compromising their superior properties, such as high power density and long cycle life [8].

Graphene oxide (GO) is a derivative of graphene that has been chemically modified with oxygen-containing functional groups such as hydroxyl, carboxyl, and epoxy groups. These functional groups enhance the water dispersibility and chemical processability of GO, enabling its use in a wide range of applications. The structural properties of GO vary depending on the degree of oxidation. The oxidation process alters the high electrical conductivity of graphene, transforming GO into a material with semiconducting characteristics. Owing to this property, GO has emerged as a key material in various fields, including sensors, energy storage systems, and environmentally friendly technologies [9–11].

Recent studies have shown that silver nanoparticles (AgNPs), owing to their advanced electrochemical and optical properties, have become highly attractive for various technological applications. Their excellent electrical conductivity enhances electron transfer within electrode materials, thereby significantly improving the electrochemical performance of nanocomposites containing AgNPs [12].

In this study, an $Ag@Ag_2O@GO$ composite was developed via a one-step hydrothermal synthesis using *Diospyros kaki* (*D. kaki*) fruit extract. To the best of our knowledge, this is the first study to report both the green synthesis of this specific composite via *D. kaki* and its electrochemical investigation for supercapacitor applications. By combining the high energy storage capability of GO with the superior conductivity of silver, this work presents a novel electrode material with unique characteristics for advanced energy storage systems.

2. EXPERIMENTAL METHOD

2.1. Materials

$AgNO_3$, $NaNO_3$, H_2SO_4, $KMnO_4$, H_2O_2, and graphite were purchased from Merck. All chemicals were of analytical grade and used for synthesis without further purification. *D. kaki* fruit was collected from Düzce/Türkiye.

2.2. Preparation of *Diospyros kaki* fruit extract

D. kaki fruit was washed with deionised water and dried at 70°C for 24 h. The dried material was then ground into a fine powder. Subsequently, 1 g of the powder was transferred into a 250 mL Erlenmeyer flask, followed by the addition of 100 mL deionised water. The mixture was heated until approximately 25 mL of the water had evaporated. After cooling to room temperature, the solution was filtered using filter paper. The obtained filtrate was stored at 4°C for use in subsequent experiments (Fig. 1).

2.3. Synthesis of graphene oxide

In the first stage of the synthesis, 5 g of graphite powder, 2.5 g of $NaNO_3$, and 115 mL of 96.4% H_2SO_4 were mixed in an ice bath and stirred for 1 hour. Then 15 g of $KMnO_4$ was gradually added to the prepared mixture while ensuring that the temperature remained below 5°C. The mixture was subsequently removed from the ice bath and stirred for 2 hours while maintaining a temperature range of 35–40°C.

In the second stage of the synthesis, 500 mL of deionized water was slowly added to the mixture, and stirring was continued for 1 hour. Afterwards, 8.4 mL of 35.7% H_2O_2 was added carefully to ensure that the temperature did not exceed 40°C, and the mixture was stirred for an additional 2 hours. During this stage, a color change from black to brown was observed. Finally, the mixture was washed with deionized water and filtered. The resulting material was dried at 100°C for 24 hours to obtain GO in powder form.

2.4. *Diospyros kaki* fruit extract-mediated hydrothermal synthesis of $Ag@Ag_2O@GO$

5 mg GO was dispersed in 10 mL of deionized water and homogenized by ultrasonication. An appropriate volume of 5 M $AgNO_3$ solution was subsequently added, and the mixture was subjected to

ultrasonication for 30 minutes to ensure uniform interaction. Following ultrasonication, a plant extract was introduced, and the synthesis was conducted hydrothermally at 60°C for 4 hours. The resulting reaction products were collected, washed three times with 20 mL of deionized water, and centrifuged at 4000 rpm for 15 minutes. Ag@Ag_2O@GO composites were prepared by freeze-drying for 24 hours in a dry ice and C_2H_3N bath to maintain at approximately − 40°C. Following this step, the remaining moisture was removed using a laboratory oven (Fig. 2). The overall formation mechanism of the nanocomposite is illustrated in Fig. 3.

As observed, *D. kaki* fruit extract acts as a reducing and capping agent during the hydrothermal process, facilitating the formation of Ag@Ag_2O nanoparticles on the GO surface.

2.5. Characterization techniques

Analytical instruments were used to determine the optical and morphological properties of the prepared AgNPs. FTIR analysis was conducted with (Perkin Elmer Spectrum Two ATR), with a range of 4000 − 500 cm^{-1}. The UV–Vis analysis of the samples was performed using a PerkinElmer WinLab-25 series spectrophotometer within the wavelength range of 200–800 nm. For powder X-ray diffraction (PXRD) analysis, a Rigaku SmartLAB diffractometer (CuK_α, 40 kV, 40 mA) was utilized. Diffraction patterns were analyzed between 5° and 80° (2θ) with a step of 0.01°. The FEI Quanta FEG 250 instrument model was used for scanning electron microscopy (SEM) analysis. Transmission electron microscopy (TEM) analysis was conducted using a JEOL JEM-1400 PLUS model instrument. For electrochemical studies, cyclic voltammetry (CV) was performed using a Metrohm 757VA potentiostat with an Ag/AgCl reference electrode and a platinum counter electrode. A 0.5-mm-diameter pencil lead (Tombow brand) served as the graphite working electrode (PGE). The supporting electrolyte was 0.5 M H_2SO_4 solution (Merck).

2.6. Preparation of Ag@Ag_2O@GO on the PGE

For electrode surface activation, PGE was immersed 0.5 cm into the working electrolyte and subjected to 5 CV cycles in 0.5 M H_2SO_4 solution at a scan rate of 100 mV s^{-1} from − 2.0 V to + 2.0 V. To create an Ag@Ag_2O@GO film on the activated PGE surface, a drop-cast technique was employed. For this purpose, 1 mg mL^{-1} Ag@Ag_2O@GO was dispersed in a 1:1 methanol:water mixture by sonication for 10 minutes. 5 µL of this dispersion was dispensed onto the activated surface at the tip of the horizontally held PGE and dried at room temperature for one minute. After this drop-cast process was repeated three times, a black thin film was observed on the PGE surface. The resulting Ag@Ag_2O@GO-coated PGE (Ag@Ag_2O@GO@PGE) was used as the working electrode, and CVs were recorded in 0.5 M H_2SO_4 solution at scan rates from 5 to 75 mV s^{-1} over the potential range from − 0.8 V to + 0.8 V.

3. RESULTS AND DISCUSSION

3.1. FT-IR and UV-Vis analyses

The FTIR spectra of GO and $Ag@Ag_2O@GO$ nanocomposite (Fig. 4) reveal the characteristic functional groups present in both structures.

The O–H stretching vibrations appear as broad bands at 3171 cm^{-1} for GO and at 3375 cm^{-1} for the nanocomposite, the latter arising from adsorbed water [13]. The C = O stretching vibrations are confirmed by the peak observed at 1715 cm^{-1} in the GO spectrum [14]. The C = C stretching vibrations associated with sp^2-hybridized and unoxidized graphitic domains are identified by the peaks at 1646 cm^{-1} in the nanocomposite and at 1608 cm^{-1} in GO [15, 16]. The O–H bending vibrations are indicated by the peak at 1419 cm^{-1} in GO [14], while the C–O stretching vibrations are represented by the peak at 1087 cm^{-1}. The peak at 819 cm^{-1} in GO corresponds to C–H bending vibrations [17], whereas the peak observed at 654 cm^{-1} in the nanocomposite is attributed to C–C vibrations [18]. Additionally, the characteristic peak at 545 cm^{-1} reflects Ag–O bond vibrations, confirming the presence of metal–oxide interactions within the nanocomposite structure [19].

The UV-Vis absorption spectrum and the corresponding plots for direct and indirect band gap energies of the synthesized $Ag@Ag_2O@GO$ nanocomposite are presented in Fig. 5.

The UV-Vis spectrum of GO exhibits a characteristic absorption peak at approximately 230 nm owing to the π-π^* transitions of aromatic C–C bonds. This corresponds to the sp^2 hybridized carbon domains. Additionally, a shoulder peak observed around 300 nm is attributed to the n-π^* transitions of oxygen-containing functional groups (C = O) [20]. In the case of the $Ag@Ag_2O@GO$ nanocomposite, the main absorption peak corresponding to the π-π^* transition is observed to be red-shifted. This shift indicates the partial reduction of GO and the restoration of the conjugated electronic structure. Furthermore, a broad absorption band emerged in the visible region at approximately 400 nm and is labeled as Ag-GO [21, 22]. This peak is attributed to the Surface Plasmon Resonance (SPR) effect of Ag nanoparticles. This observation provides strong evidence for the successful anchoring of Ag species onto the GO sheets and suggests the material's potential as a visible-light-active photocatalyst. The optical band gap energies were determined using the Tauc equation $(ahv)^n = K(hv - E_g)$ [23]. In this regard, the values n = 2 and n = 1/2 were used to analyze the allowed direct and indirect transitions, respectively. First, the direct band gap energies were estimated from the $(ahv)^2$ plots. Accordingly, the direct band gap of GO was calculated to be 3.93 eV [24] while for $Ag@Ag_2O@GO$ nanocomposite, it was found to be 3.84 eV. Subsequently, the indirect band gap energies were derived using the $(ahv)^{1/2}$ relation. The indirect band gap values for GO and the nanocomposite were determined to be 2.04 eV [25, 26] and 3.94 eV, respectively [23]. These results provide insight into the electronic properties and defect states of the synthesized materials.

3.2. PXRD analyses

The structural properties of $Ag@Ag_2O@GO$ nanocomposite were investigated using PXRD analysis (Fig. 6).

In the analysis results, while the characteristic (001) plane of the pure GO structure is observed at 10.35° [27], a decrease in the intensity of this peak is noted in the nanocomposite structure. Characteristic peaks belonging to the face-centered cubic (FCC) structure of metallic Ag were detected at 38.06, 44.23, 64.35, and 77.28°, these values correspond to the (111), (200), (220), and (311) Miller indices, respectively, and are in agreement with JCPDS No. 01-087-0720. Similarly, reflections belonging to the cubic Ag_2O phase were observed at 27.76, 32.16, and 46.14°, and these peaks were attributed to the (110), (111), and (211) crystal planes, respectively. The positions of the Ag_2O peaks are in full agreement with the JCPDS No. 01-76-1393 [28], demonstrating that both Ag and Ag_2O nanostructures were successfully synthesized on the GO surface.

3.3. Morphological studies

The surface morphology and elemental composition of the synthesized materials were investigated using SEM-EDX and TEM techniques (Fig. 7).

Upon examination of the SEM images of the pristine GO structures (Fig. 7a,b), the crumpled, folded, and stacked layered morphology with a large surface area—a characteristic feature of GO—is clearly observed [29]. This undulating 3-dimensional structure provides an ideal matrix for the anchoring and distribution of nanoparticles on the surface.

Significant morphological alterations were observed on the surface of the GO sheets in the SEM images of $Ag@Ag_2O@GO$ nanocomposite, as depicted in Fig. 7(c, d). In contrast to the pristine GO surface, bright spots exhibiting spherical morphology and homogeneous distribution over the carbon sheets are evident in the composite structure. According to the atomic number contrast (Z-contrast) principle in SEM [2, 30]. The fact that Ag—being a heavier element than carbon—possesses a higher backscattered electron (BSE) yield in these regions confirms that the bright areas correspond to Ag and Ag_2O nanoparticles.

The EDX analysis, conducted to verify the chemical purity and elemental composition of the nanocomposite, is presented in Fig. 7 (e). Only characteristic peaks corresponding to C, O, and Ag were detected in the spectrum, revealing a weight percentage (wt%) distribution of 33.1%, 28.6%, and 38.4%, respectively. The substantial oxygen content corroborates the presence of both graphene oxide functional groups and the Ag_2O phase within the structure. The absence of any impurity peaks in the spectrum indicates that the synthesis process was carried out with high purity.

The TEM image, which provides more detailed insight into the internal structure and particle size distribution of the material, is shown in Fig. 7(f, g, h). The image clearly reveals the presence of dark-contrast nanoparticles on the semi-transparent, thin graphene oxide sheets. Corroborating the SEM findings, the TEM analysis confirms that the $Ag@Ag_2O$ nanoparticles are homogeneously distributed on the GO surface with minimal agglomeration [31].

3.4. Electrochemical properties and capacitance performances

The electrochemical properties of $Ag@Ag_2O@GO$ were examined by CV at different scan rates, as shown in Fig. 8.

Figure 8. Voltammograms recorded by CV in 0.5 M H_2SO_4 aqueous electrolyte using PGE at scan rates of 5–75 mV/s, GO (a), $Ag@Ag_2O@GO$ (b), and specific capacitance values of GO, $Ag@Ag_2O@GO$ at scan rates of 5, 25, 50, 75 mV/s (c).

In Fig. 8a, the anodic (0.4 V) and cathodic (0.3 V) peaks of GO were assigned to the redox pair of electrochemically active oxygen-containing groups on the surface [32]. In the CV of the $Ag@Ag_2O@GO$ composite, these GO-related peaks were also observed at approximately the same potentials (Fig. 8b). The reduction peak at 0.3 V was attributed to the reduction of GO to reduced-GO [32]. In addition, the CV of the composite showed additional oxidation and reduction peaks at 0.18 V and 0.02 V, respectively (Fig. 8b). These additional peaks were attributed to the oxidation and reduction of Ag^0 and Ag^+, respectively [33].

Figure 8 (c) displays the scan rate-dependent specific capacitance (C_s) of GO and $Ag@Ag_2O@GO$ electrodes at 5, 25, 50, and 75 mV s^{-1}. The C_s values were derived from the CV data utilizing Eq. (1) [2, 34].

$$\mathrm{C_s} = \frac{\int_{V_i}^{V_f} I\,(\mathrm{v})}{m \times v_s \times \Delta\,\mathrm{V}}$$

1

In this equation, C_s denotes the specific capacitance of the electrode (F g^{-1}), while *I* and *m* represent the current density (A cm^{-2}) and the mass loading of the active material (g), respectively. Furthermore, v_s denotes the scan rate (V s^{-1}), and ΔV denotes the potential window (V_f - V_i), defined by the initial (V_i) and final (V_f) potential limits.

Based on the calculations performed using this equation, the C_s values for both electrodes were found to decrease with increasing scan rates, as expected, due to the diffusion-limited access of electrolyte ions to the inner active sites [35]. The GO electrode exhibited specific capacitance values of 58.3, 47.2, 42.1, and 38.9 F g^{-1}, respectively. In contrast, $Ag@Ag_2O@GO$ nanocomposite demonstrated significantly superior electrochemical performance, yielding specific capacitance values of 125.5, 69.1, 59.1, and 58.6 F g^{-1} at the corresponding scan rates. Notably, at the lowest scan rate of 5 mV s^{-1}, the composite achieved a maximum specific capacitance of 125.5 F g^{-1}, which represents a more than two-fold enhancement compared to GO (58.3 F g^{-1}). Furthermore, even at a high scan rate of 75 mV s^{-1}, the

composite retained a capacitance of 58.6 F g^{-1}, surpassing the maximum capacitance of GO measured at 5 mV s^{-1}. This substantial improvement is attributed to the synergistic effect of $Ag@Ag_2O$ nanoparticles, which enhance the electrical conductivity and facilitate rapid electron transfer within the GO matrix.

4. CONCLUSION

In this study, an eco-friendly $Ag@Ag_2O@GO$ nanocomposite was successfully synthesized via a one-step hydrothermal method utilizing *Diospyros kaki* fruit extract as a dual reducing and stabilizing agent. The structural, morphological, and electrochemical properties of the synthesized nanocomposite were comprehensively characterized using FT-IR, UV-Vis, PXRD, SEM-EDX, TEM, and CV techniques. FT-IR spectral analysis confirmed the presence of functional groups within the composite structure and demonstrated the successful establishment of metal-oxide interactions, specifically evidenced by the Ag-O bond observed at 545 cm^{-1}. Furthermore, UV-Vis results corroborated the formation of Ag nanoparticles via the Surface Plasmon Resonance (SPR) band around 400 nm, while the red-shift at the absorption edge confirmed the partial reduction of the graphene oxide structure. Additionally, calculations based on the Tauc method determined the direct band gap energies of GO and $Ag@Ag_2O@GO$ nanocomposite to be 3.93 eV and 3.84 eV, respectively, while the indirect band gap energies were found to be 2.04 eV and 3.94 eV. These optical modifications indicate a reorganization of the material's electronic structure upon the formation of the nanocomposite. $Ag@Ag_2O@GO$ nanocomposite exhibited a maximum specific capacitance of 125.5 F g^{-1} at a scan rate of 5 mV s^{-1}, which is more than double the capacitance of 58.3 F g^{-1} obtained for pure GO. This enhancement is attributed to the synergistic effect of $Ag@Ag_2O$ nanoparticles, which significantly improve the electrical conductivity and electron transfer rates within the electrode material. Furthermore, the composite retained a high capacitance of 58.6 F g^{-1} even at a higher scan rate of 75 mV s^{-1}, surpassing the maximum performance of pure GO. These results demonstrate that the *Diospyros kaki* assisted green synthesis offers a sustainable, low-cost, and effective strategy for developing advanced electrode materials, thereby presenting a promising avenue for green nanotechnology to satisfy the growing demand for high-performance supercapacitor applications.

Declarations

Ethical approval

Not Applicable.

Use of generative AI and AI-assisted technologies

There is no generative AI and AI-assisted technologies usage to declare.

Conflict of interest

There is no conflict of interest to declare.

Funding

The authors declare that no funds, grants, or other support were received during the preparation of this manuscript.

Author Contribution

Ayşe Bütün: Material preparation, Formal analysis, Investigation, Data curation, Writing–original draft, Kübra Zenkin: Material preparation, Formal analysis, Investigation, Data curation, Writing –original draft, Deniz Emre: Formal analysis, Investigation, Data curation, Visualization, Sefa Durmuş: Conceptualization, Methodology, Writing – review & editing, Project administration, Funding acquisition, Supervision, Selehattin Yılmaz: Conceptualization, Methodology, Writing – review & editing, Supervision.

Data Availability

The data used and/or analyzed during the current study are available from the corresponding author on reasonable request

References

1. Niraj K, Su-Bin K, Seul-Yi L, Soo-Jin P (2022) Recent advanced supercapacitor: a review of storage mechanisms, electrode materials, modification, and perspectives. Nanomaterials 12:20. https://doi.org/10.3390/nano12203708
2. Kübra Z, Sefa D, Deniz E, Ali B, Selehattin Y (2025) *Salvia officinalis* leaf extract-stabilized NiO NPs, ZnO NPs, and NiO@ZnO nanocomposite: Green hydrothermal synthesis, characterization and supercapacitor application. Biomass Convers Biorefinery 15:7:10149–10164. https://doi.org/10.1007/s13399-024-05808-7
3. Jie Z, Min. G, Xi C (2023) Supercapacitors for renewable energy applications: A review. Micro Nano Eng 21:100229. https://doi.org/10.1016/j.mne.2023.100229
4. Mayank P et al (2024) High energy density supercapacitors: an overview of efficient electrode materials, electrolytes, design, and fabrication. Chem Rec 24:e202300236. https://doi.org/10.1002/tcr.202300236
5. Mustafa Ergin Ş, Frede B, Ariya S (2022) A comprehensive review on supercapacitor applications and developments. Energies 15:3. https://doi.org/10.3390/en15030674

6. Zhenhong F (2025) A review of recent advances in supercapacitors: materials, electrolytes, and device engineering. JCEIM 19(3):17–24. https://doi.org/10.54097/afs0y104
7. Thibeorchews P et al (2021) Pseudocapacitors, Supercapacitors for the Next Generation. IntechOpen. https://doi.org/10.5772/intechopen.98600
8. Lili G et al (2025) Recent advances and challenges in hybrid supercapacitors based on metal oxides and carbons. Inorganics 13:2. https://doi.org/10.3390/inorganics13020049
9. Da C, Hongbin F, Jinghong L (2012) Graphene oxide: preparation, functionalization, and electrochemical applications. Chem Rev 112(11):6027–6053. https://doi.org/10.1021/cr300115g
10. Dimitrios GT et al (2021) Graphene oxide synthesis, properties and characterization techniques: A comprehensive review. ChemEngineering 5:364. https://doi.org/10.3390/chemengineering5030064
11. Seyyed Mojtaba M et al (2023) Recent advances in energy storage with graphene oxide for supercapacitor technology. Sustain Energy Fuels 7:21:5176–5197. https://doi.org/10.1039/d3se00867c
12. Zafer Ç, Nuray Y (2019) The effect of Ag loading on supercapacitor performance of graphene based nanocomposites. Fuller Nanotub Car N 27(1):65–76. https://doi.org/10.1080/1536383X.2018.1504022
13. Hüseyin Ö et al (2023) Biosynthesis and characterization of α-FeOOH nanoparticles using Isabella grape (Vitis Labrusca L.) extract. Turkish J Anal Chem 5(1):43–49. https://doi.org/10.51435/turkjac.1306657
14. Viet HL et al (2020) Fabrication and electrochemical behavior investigation of a pt-loaded reduced graphene oxide composite (Pt@rGO) as a high-performance cathode for dye-sensitized solar cells. Int J Photoenergy 2020:1. https://doi.org/10.1155/2020/8927124
15. Deepak S et al (2015) silver imprinted graphene nanocomposites: synthesisis and morphological study. Appl Sci Adv Mater Int 1:6, 224 – 27.
16. Rachida D, Touffik B, Samir B (2019) Influence of functionalized reduced graphene oxide and compatibilizer on mechanical, thermal and morphological properties of polypropylene/polybutene-1 (PP/PB-1) blends. J Adhes Sci Technol 33(16):1729–1757. https://doi.org/10.1080/01694243.2019.1611367
17. Meng-meng C et al (2019) Synthesis of graphene oxide/polyacrylamide composite membranes for organic dyes/water separation in water purification. J Mater Sci, 54:1, 252–264, 2019. https://doi.org/10.1007/s10853-018-2828-9
18. Iman S et al (2018) Thermal reduction of graphene oxide: How temperature influences purity. J Mater Res 33:23:4113–4122. https://doi.org/10.1557/jmr.2018.338
19. Parmeshwar LM et al (2023) Ag_2O-adorned ZnO nanostructures: cooperative and sustainable nanomaterial system for effective reduction and mineralization of hazardous water pollutants. Environ Sci Pollut Res 30:26:68770–68791. https://doi.org/10.1007/s11356-023-27215-7
20. Muhammad I et al (2020) Hydrothermal synthesis of silver decorated reduced graphene oxide (rGO) nanoflakes with effective photocatalytic activity for wastewater treatment. Nanoscale Res Lett

15:195. https://doi.org/10.1186/s11671-020-03323-y

21. Vinay SP et al (2020) Facile combustion synthesis of Ag_2O nanoparticles using cantaloupe seeds and their multidisciplinary applications. Appl Organomet Chem 34:10e5830. https://doi.org/10.1002/aoc.5830
22. Nisreen A et al (2021) Ag/AgO nanoparticles: Green synthesis and investigation of their bacterial inhibition effects. Mater Today Proc 45(6):5788–5792. https://doi.org/10.1016/j.matpr.2021.03.166
23. Salah EL et al (2021) Catalytic activity for dye degradation and characterization of silver/silver oxide nanoparticles green synthesized by aqueous leaves extract of *Phoenix dactylifera* L. Res Sq 18:1–26
24. Salmansur MA et al (2020) Investigating the structural, optical and antibacterial properties of GO, GO:Ag, GO:ZnO thin layers and GO:ZnO/GO:Ag bilayers synthesized by spray pyrolysis method. Iran J Mater Sci Eng 17(4):170–181. https://doi.org/10.22068/ijmse.17.4.170
25. Karina B et al (2015) Photocatalytic activity in phenol removal of water from graphite and graphene oxides: Effect of degassing and chemical oxidation in the synthesis process. J Chem 2015:1. https://doi.org/10.1155/2015/254631
26. Komal B et al (2020) Synthesis of graphene oxide with a lower band gap and study of charge transfer interactions with perylenediimide. New J Chem 44:29, 12704–12714. https://doi.org/10.1039/d0nj01906b
27. Pavel AM et al (2019) Synthesis and characterization of polyethylene terephthalate-reduced graphene oxide composites. IOP Conf Ser Mater Sci Eng 693:1. https://doi.org/10.1088/1757-899X/693/1/012036
28. Manel A et al (2024) Plant extract-mediated synthesis of Ag/Ag_2O nanoparticles using *Olea europaea* leaf extract: assessing antioxidant, antibacterial, and toxicological properties. Biomass Convers Biorefinery 14:24:31309–31322. https://doi.org/10.1007/s13399-023-05093-w
29. Kelsey H et al (2022) Crumpled graphene oxide for enhanced room temperature gas sensing: understanding the critical roles of surface morphology and functionalization. J Mater Chem A 11(1):447–459. https://doi.org/10.1039/d2ta06883d
30. Joseph G et al (2017) Scanning Electron Microscopy and X-ray Microanalysis, 4th edn. Springer, New York
31. Rama L, Balavijayalakshmi J (2018) Silver nanocomposites decorated reduced graphene oxide nanosheets for electrochemical sensor applications. Orient J Chem 34(6):2872–2877. https://doi.org/10.13005/ojc/340626
32. Liuyun C et al (2011) Direct electrodeposition of reduced graphene oxide on glassy carbon electrode and its electrochemical application. Electrochem commun 13:2:133–137. https://doi.org/10.1016/j.elecom.2010.11.033
33. Santanu D et al (2021) Surfactant-free synthesis of carbon-supported silver (Ag/C) nanobars as an efficient electrocatalyst for alcohol tolerance and oxidation of sodium borohydride in alkaline medium. SN Appl Sci 3(6):617. https://doi.org/10.1007/s42452-021-04601-9

34. Muhammad MI et al (2019) Facile preparation of Mn_3O_4/rGO hybrid nanocomposite by sol–gel in situ reduction method with enhanced energy storage performance for supercapacitor applications. J Sol-Gel Sci Technol 93(3):703–713. https://doi.org/10.1007/s10971-019-05184-z
35. Saad MJ et al (2023) Hydrated and non-hydrated rGO-$MnMoO_4$ nanocomposites as supercapacitor electrodes. Ionics 29(10):4263–4273. https://doi.org/10.1007/s11581-023-05142-4

Figures

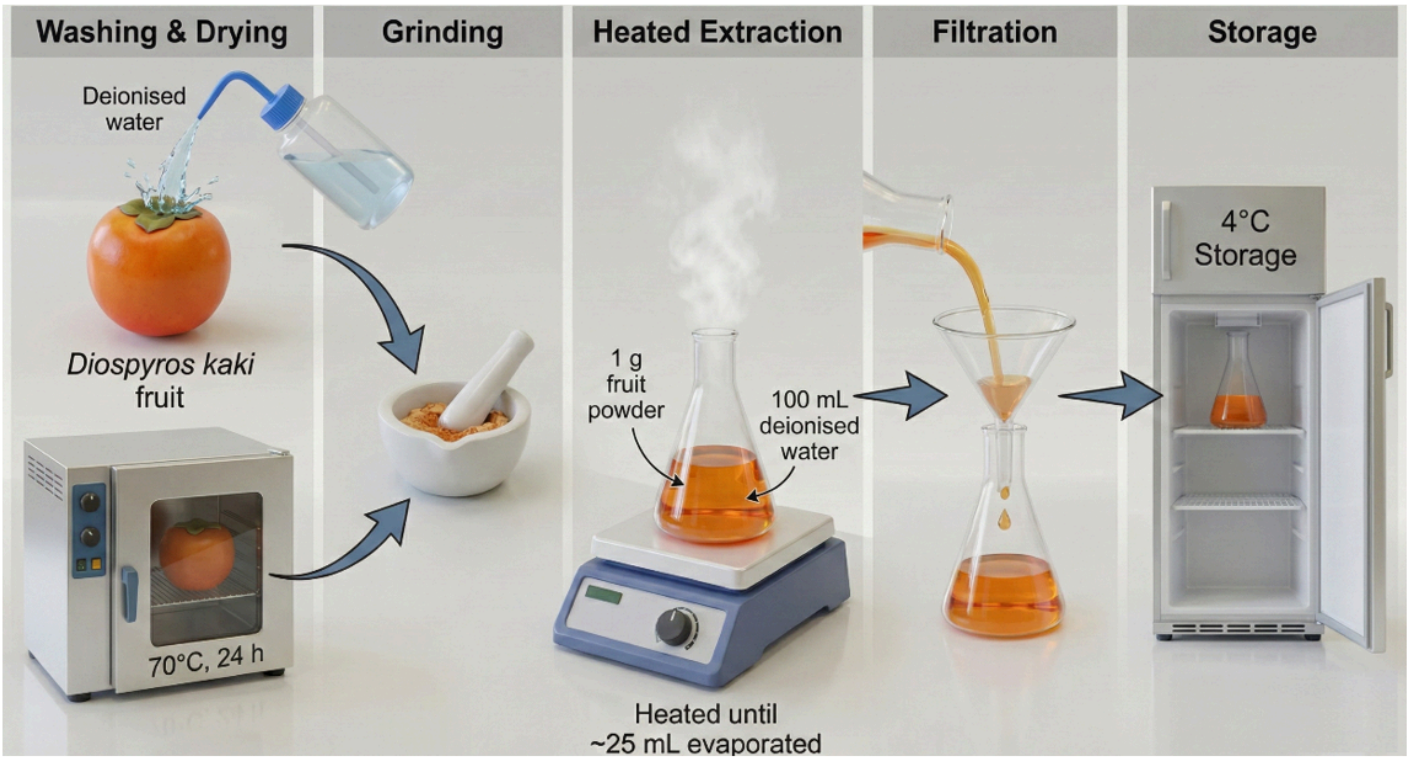

Figure 1

Schematic illustration of the extraction procedure of *Diospyros kaki* fruit extract.

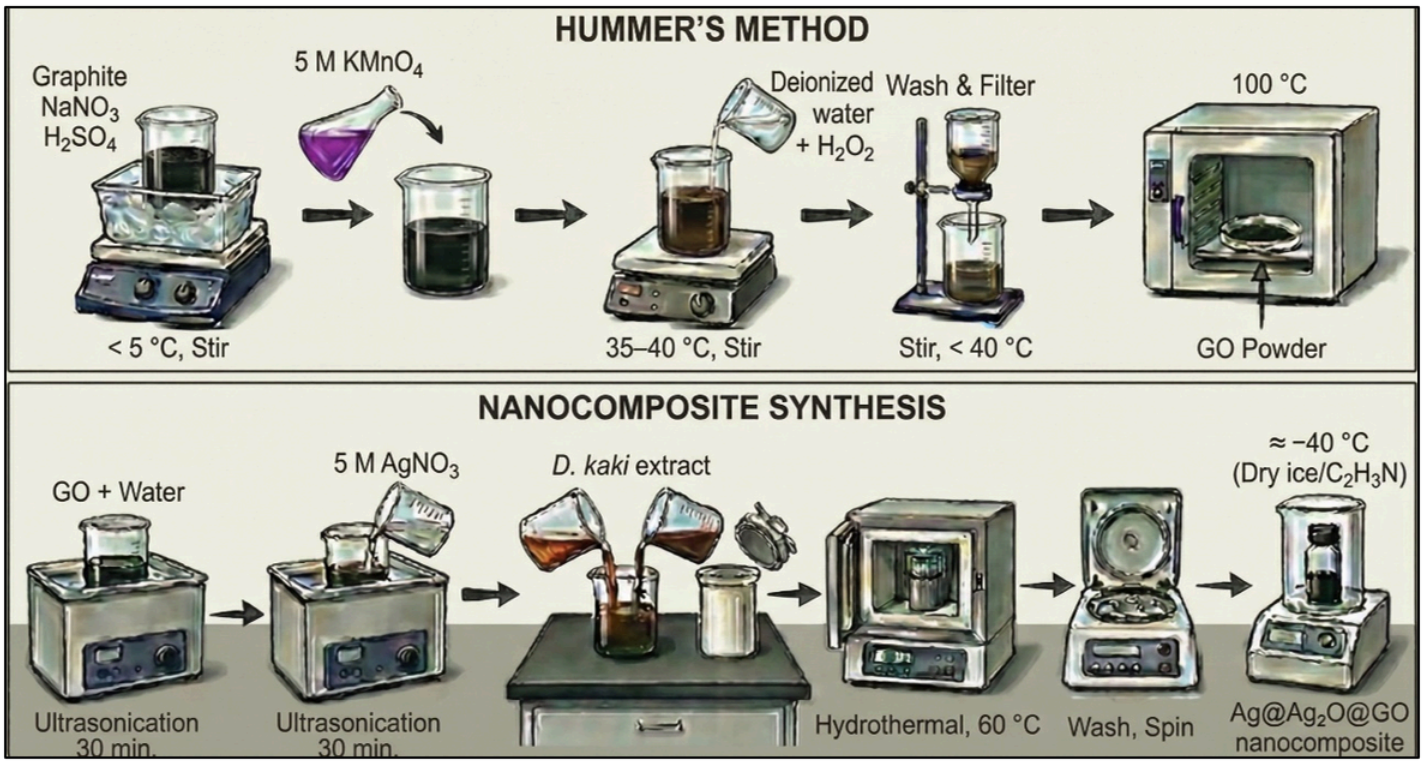

Figure 2

Schematic representation of the procedure followed for nanocomposite synthesis.

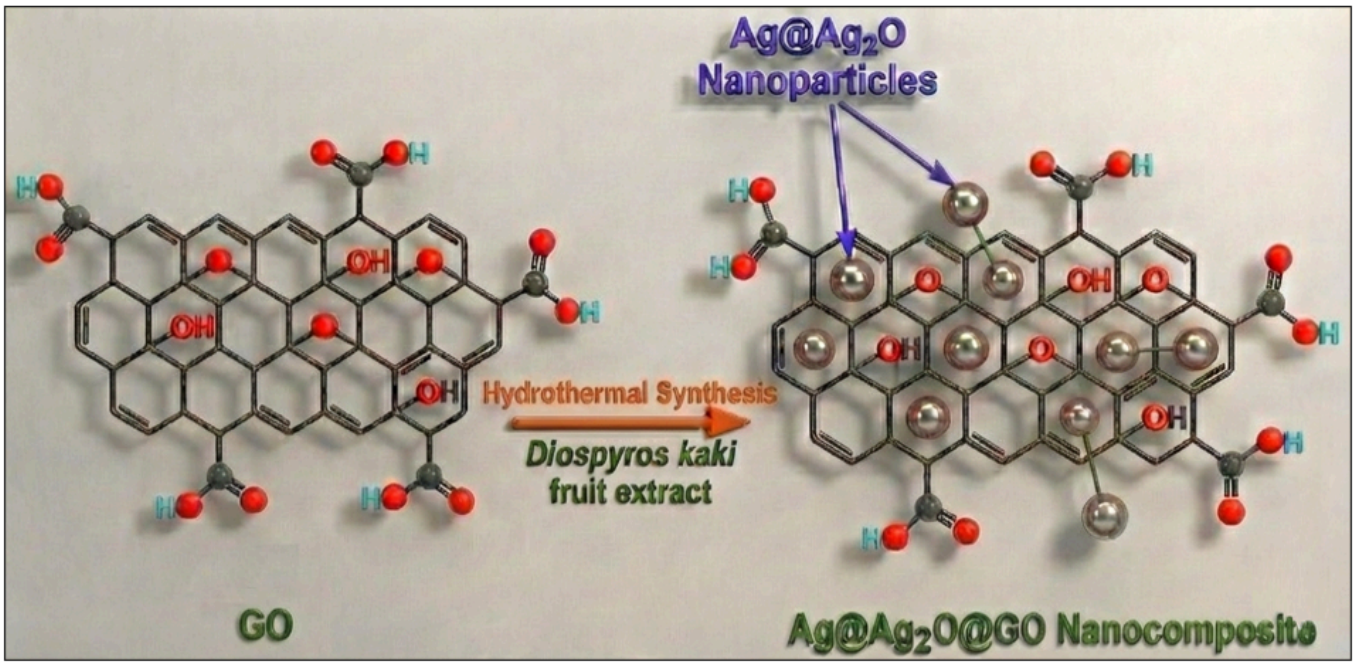

Figure 3

Hydrothermal preparation of $Ag@Ag_2O@GO$ nanocomposites via *D. kaki* extract.

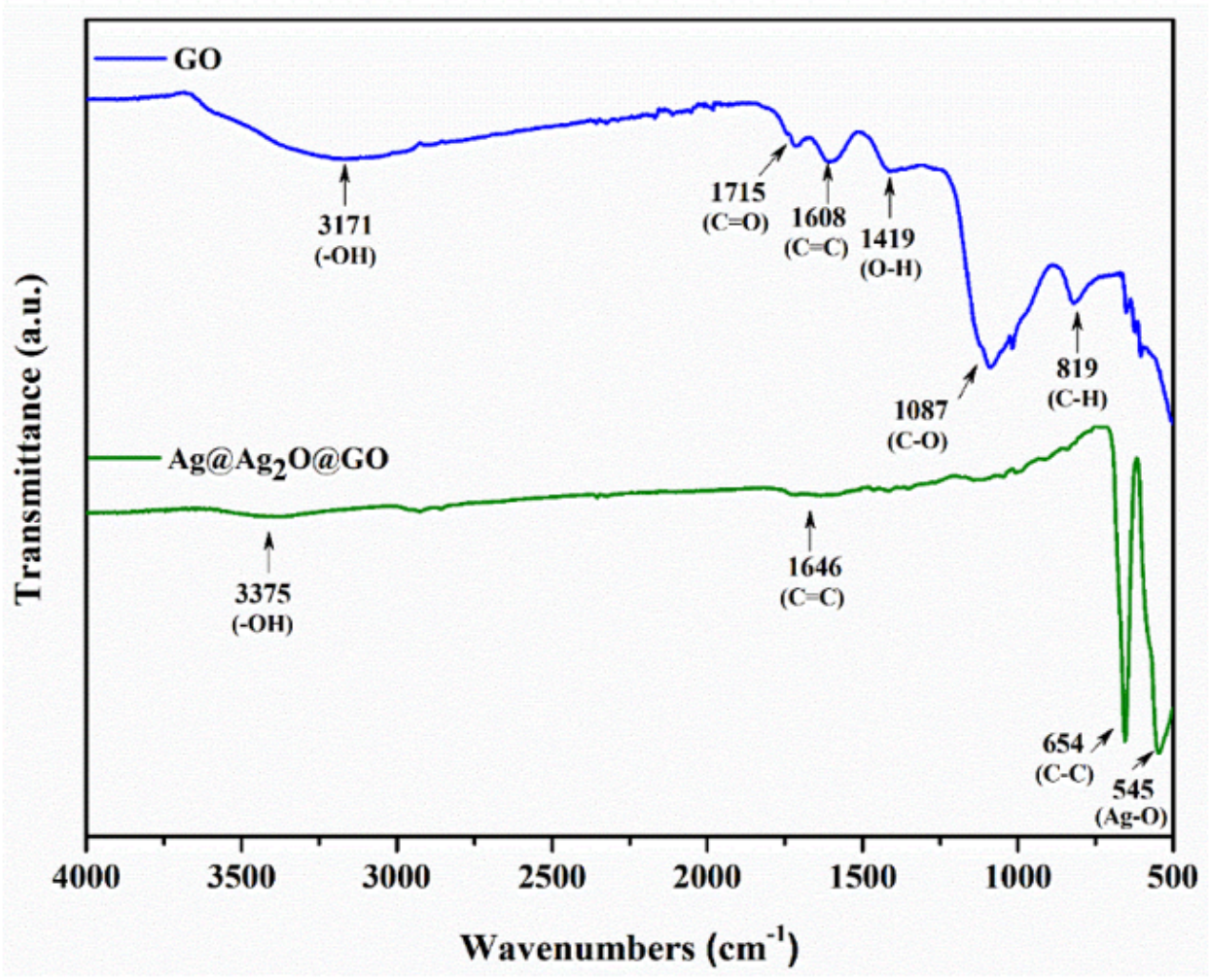

Figure 4

FTIR spectra of GO and $Ag@Ag_2O@GO$ nanocomposite.

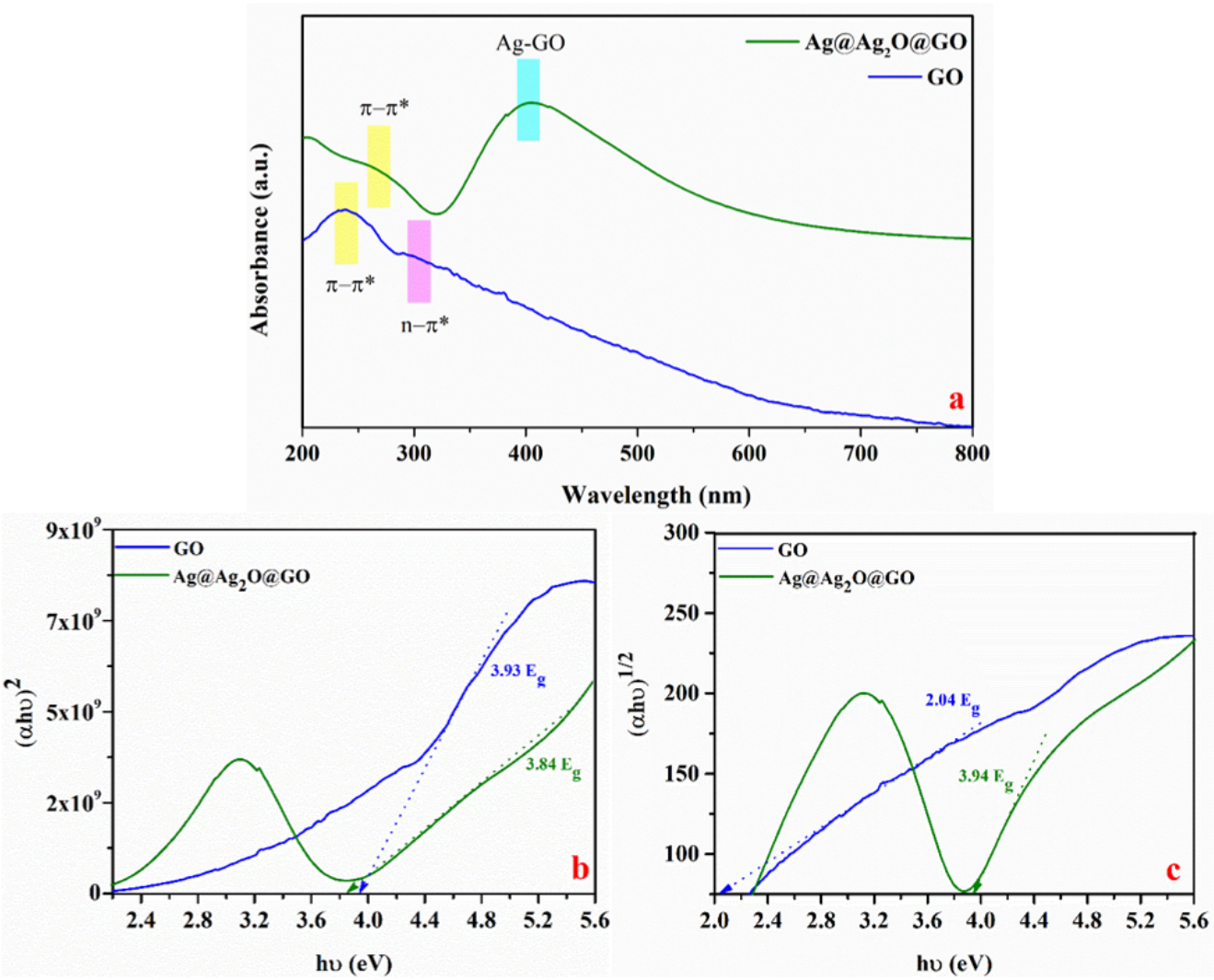

Figure 5

(a) UV-Vis absorption spectra and Tauc plots for (b) direct and (c) indirect band gap of GO and $Ag@Ag_2O@GO$ nanocomposites.

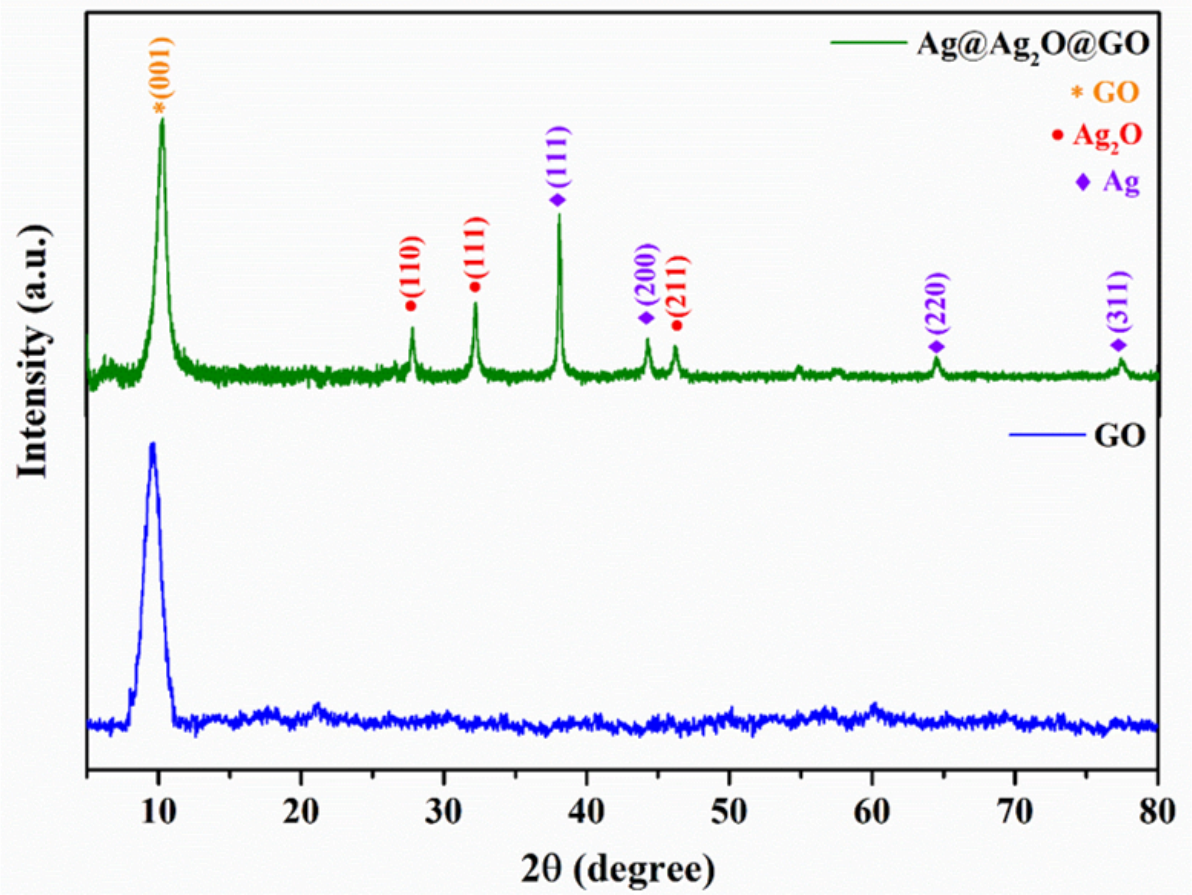

Figure 6

PXRD patterns of GO and $Ag@Ag_2O@GO$ nanocomposite.

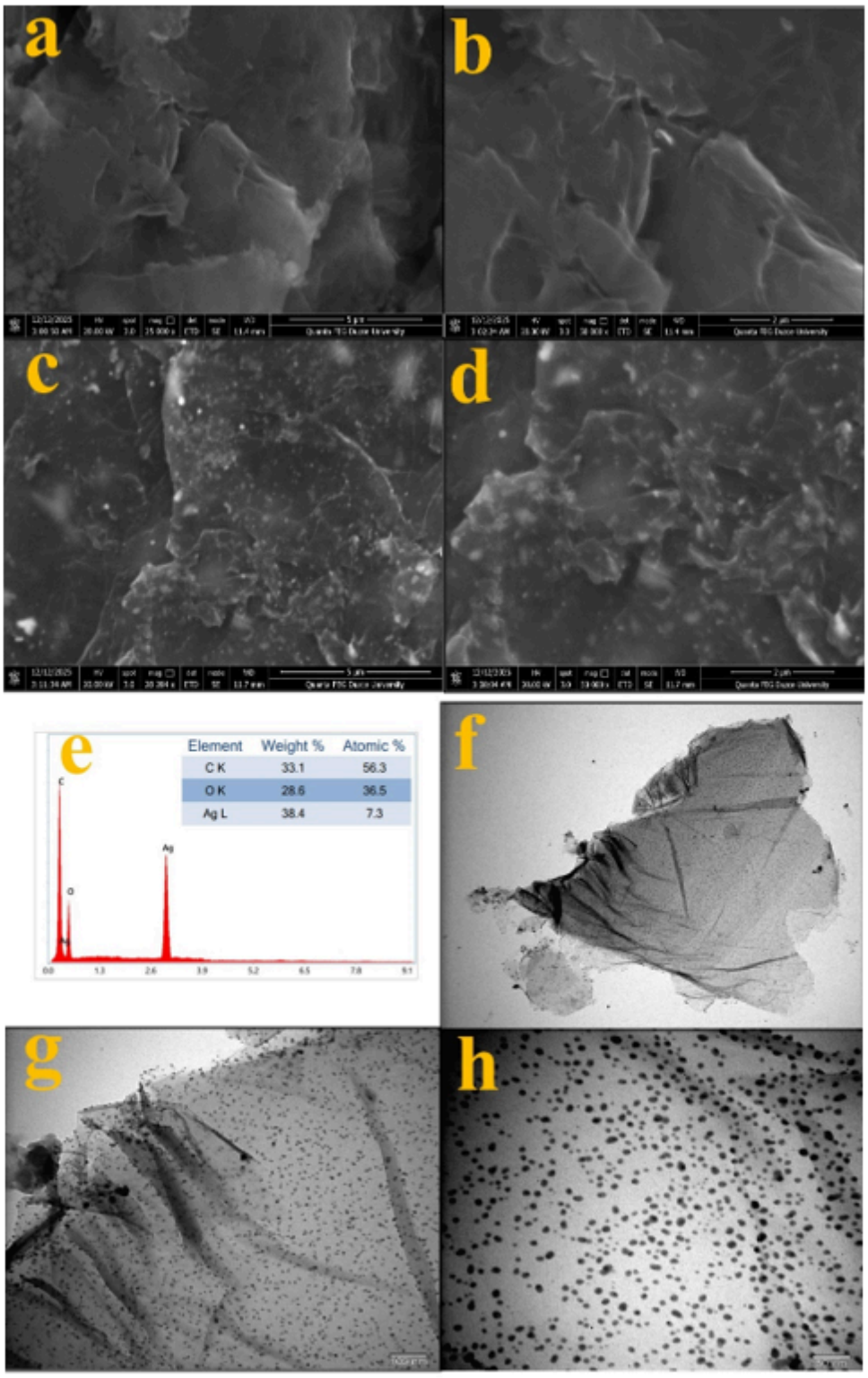

Figure 7

SEM images of GO (a,b) and SEM images (c,d), EDX spectrum (e), and TEM images (f–h) corresponding to Ag@Ag_2O@GO nanocomposite.

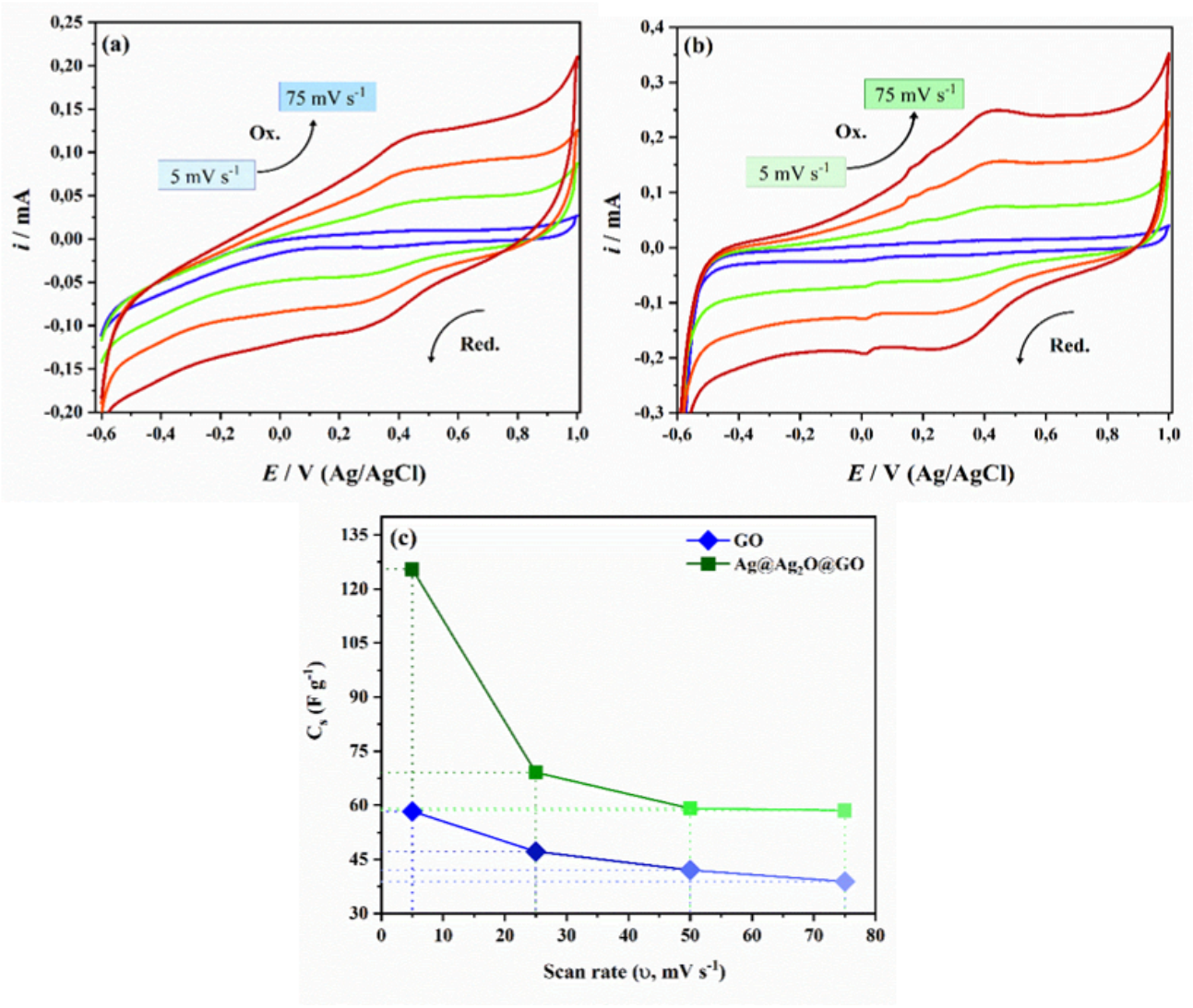

Figure 8

Voltammograms recorded by CV in 0.5 M H_2SO_4 aqueous electrolyte using PGE at scan rates of 5–75 mV/s, GO (a), Ag@Ag_2O@GO (b), and specific capacitance values of GO, Ag@Ag_2O@GO at scan rates of 5, 25, 50, 75 mV/s (c).